

Winter 2018

Dialkynylborane Complexes of Formazanate Ligands: Synthesis, Electronic Properties, and Reactivity

Alex Van Belois

Ryan R. Maar

Mark S. Workentin

Joe Gilroy
jgilroy5@uwo.ca

Follow this and additional works at: <https://ir.lib.uwo.ca/chempub>

 Part of the [Chemistry Commons](#)

Citation of this paper:

Van Belois, Alex; Maar, Ryan R.; Workentin, Mark S.; and Gilroy, Joe, "Dialkynylborane Complexes of Formazanate Ligands: Synthesis, Electronic Properties, and Reactivity" (2018). *Chemistry Publications*. 98.
<https://ir.lib.uwo.ca/chempub/98>

Dialkynylborane Complexes of Formazanate Ligands: Synthesis, Electronic Properties, and Reactivity

Alex Van Belois, Ryan R. Maar, Mark S. Workentin*, and Joe B. Gilroy*

Department of Chemistry and the Centre for Advanced Materials and Biomaterials Research
(CAMBR), The University of Western Ontario, London, Ontario, Canada, N6A 5B7.

ABSTRACT

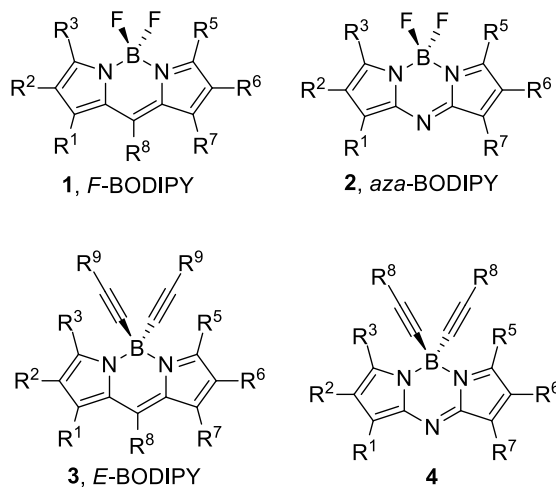
Dialkynylborane complexes of *N*-donor ligands have received significant attention due to their application in biological imaging, as light-harvesting materials, and as the functional component of organic photovoltaics. Despite these advances, relatively few types of *N*-donor ligands have been explored in this context. To this end, we prepared a series of dialkynylborane complexes of formazanate ligands and explored their electronic properties and reactivity. In doing so, we demonstrated that: 1) The nature of the alkynyl substituents has little influence over the UV-vis absorption properties of the title complexes, but does affect the potentials at which they are electrochemically oxidized and reduced. 2) Dialkynylborane formazanate complexes can be converted to stable radical anions by chemical reduction with cobaltocene derivatives. 3) Copper-assisted alkyne-azide cycloaddition chemistry at the alkynyl substituents directly bound to boron can be used to elaborate structural diversity. These conclusions are likely to lead to the development of, and provide guiding principles for the design of, future examples of functional molecular materials based on boron complexes of *N*-donor ligands.

INTRODUCTION

Fluoride-substituted boron dipyrromethenes (*F*-BODIPYs, **1**), which benefit from structural rigidity and advantageous push-pull electronics due to the presence of the boron difluoride (BF₂) moiety, are one of the most widely studied classes of molecular dyes and have seen extensive use as fluorescence probes and imaging agents.¹⁻⁴ One of the most attractive features of their chemistry is the ability to tune the absorption and emission properties through structural variation of the dipyrromethene scaffold at the R¹-R⁸ positions, or by incorporation of a third nitrogen atom in the ligand framework to form *aza*-BODIPYs (**2**). Despite the widespread

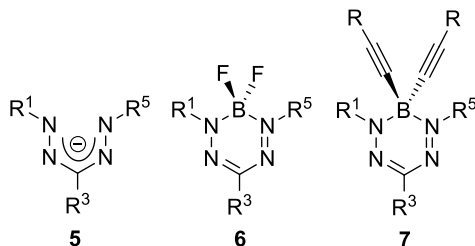
use of such structural modification strategies, the synthesis of BODIPYs and their modification can be synthetically challenging, low-yielding, and expensive.

In an effort to circumvent some of these challenges, Ziessel and co-workers produced the first examples of dialkynylborane complexes of dipyrromethenes (*E*-BODIPYs, **3**) in the mid-2000s,⁵⁻⁶ which can be prepared via the reaction of *F*-BODIPYs with the lithium salts of substituted alkynes. Over the past decade, the chemistry of *E*-BODIPYs and related compounds derived from *aza*-BODIPYs (**4**) has expanded significantly⁷⁻¹³ and these compounds have been used extensively as light-harvesting arrays¹⁴⁻¹⁷ and dye lasers,¹⁸⁻¹⁹ in biological imaging,²⁰⁻²⁴ as the functional component of photovoltaic cells,²⁵⁻²⁸ and as building blocks for functional assemblies.²⁹⁻³⁷ Given these advances, it may be surprising that dialkynylborane complexes of relatively few classes of *N*-donor ligands have been explored to date.



Recently, transition metal complexes of formazanate ligands (**5**) have received significant attention³⁸⁻⁵² and their BF₂ complexes (**6**) have emerged as attractive alternatives to *F*-BODIPYs as a result of their relatively straightforward and inexpensive syntheses and their tuneable absorption/emission and redox properties.⁵³⁻⁵⁹ As a result, the latter have found application as cell-imaging agents,^{56,59} electrochemiluminescence (ECL) emitters,⁶⁰⁻⁶¹ precursors to a wide

range of unusual BN heterocycles,⁶²⁻⁶³ building blocks for multifunctional polymers,⁶⁴⁻⁶⁷ and to promote N-H and N-C bond homolysis.⁶⁸



Herein, we build on previous reports describing the effects of substituent variation at the formazanate backbone^{54-55,58,69} by synthesizing the first examples of alkynylborane complexes of formazanate ligands (**7**) and studying their electronic properties and reactivity. These complexes represent the first discrete boron adducts of formazanate ligands prepared by the substitution of the fluorine atoms of BF₂ formazanates.

EXPERIMENTAL SECTION

General Considerations

Solvents were obtained from Caledon Laboratories, dried using an Innovative Technologies Inc. solvent purification system, collected under vacuum, and stored under an N₂ atmosphere over 4 Å molecular sieves. All other reagents were purchased from Sigma Aldrich, Alfa Aesar or Oakwood Chemical and used as received. 1,3,5-tri-*p*-tolylformazan **8** was prepared according to a literature procedure.⁷⁰ NMR spectra were recorded on a Bruker 400 MHz NMR spectrometer, 400 MHz Varian INova NMR spectrometer, or 600 MHz Varian Inova NMR spectrometer. ¹H NMR spectra were recorded in CDCl₃ or CD₂Cl₂ and referenced against residual protonated solvent at 7.27 and 5.32 ppm, respectively. ¹³C{¹H} NMR spectra were referenced to CDCl₃ at 77.0 ppm. ¹¹B NMR spectra were referenced internally to BF₃•OEt₂ at 0 ppm. ¹⁹F NMR spectra

were referenced internally to CFCl_3 at 0 ppm. Mass spectra were recorded in positive-ion or negative-ion mode using a Bruker microTOF II electrospray ionization spectrometer. UV-vis absorption spectra were recorded using a Cary 5000 Scan instrument using standard quartz cells (1 cm path length) with a scan range of 200 to 1200 nm. Samples were dissolved in spectroscopic grade solvents to obtain various concentrations. The background was subtracted from each spectrum and the solvent used for each experiment is indicated. FT-IR spectra were recorded using a Perkin Elmer Spectrum Two FT-IR spectrometer.

Cyclic Voltammetry

Cyclic voltammetry experiments were performed using a Bioanalytical Systems Inc. (BASi) Epsilon potentiostat and analyzed using BASi Epsilon software. Typical electrochemical cells consisted of a three-electrode setup including a glassy carbon working electrode, platinum counter electrode, and silver *pseudo* reference electrode. Experiments were run at 50–1000 mV s^{-1} in degassed CH_2Cl_2 solutions of the analyte (~1 mM) and electrolyte (0.1 M $[\text{nBu}_4\text{N}][\text{PF}_6]$). Cyclic voltammograms were internally referenced against the ferrocene/ferrocenium redox couple (~1 mM internal standard) and corrected for internal cell resistance using the BASi Epsilon software. The CV obtained for complex **10d** was referenced against the ferrocene/ferrocenium redox couple using decamethylferrocene/decamethylferrocenium (–520 mV vs ferrocene/ferrocenium under identical conditions) as an internal reference.

Electron Paramagnetic Resonance (EPR) Spectroscopy

EPR measurements were made for degassed 10 μM THF solutions of radical anions **10a \cdot^-** and **10d \cdot^-** using a JEOL JES-FA200 EPR spectrometer. All measurements were made at 21 °C and *g*-factors were referenced relative to a built-in Mn^{2+} marker within the resonant cavity of the

instrument.

BF₂ Complex 9: Under N₂, formazan **8** (1.0 g, 3.0 mmol) was dissolved in dry toluene (100 mL). NEt₃ (1.4 mL, 10 mmol) was then added dropwise and the solution was stirred for 5 min. BF₃•OEt₂ (1.9 mL, 15 mmol) was then added, and the solution was heated at 80 °C for 18 h. The solution changed from dark red to dark purple during this time. The solution was then cooled to room temperature and H₂O (20 mL) was added to quench any reactive boron-containing compounds. The solution was then washed with deionized H₂O (3 × 50 mL), dried over MgSO₄, gravity filtered and concentrated *in vacuo*. The resulting residue was purified by flash chromatography (CH₂Cl₂, neutral alumina) to afford the BF₂ complex **9** as a dark purple microcrystalline solid after solvent removal *in vacuo*. Yield = 0.98 g (86%). M.p. 166–168 °C. ¹H NMR (399.8 MHz, CDCl₃): δ 7.99 (d, ³J_{HH} = 8 Hz, 2H, Aryl CH), 7.80 (d, ³J_{HH} = 8 Hz, 4H, Aryl CH), 7.29–7.26 (m, 6H, Aryl CH), 2.43 (s, 3H, CH₃), 2.42 (s, 6H, CH₃). ¹¹B NMR (128.3 MHz, CDCl₃): δ -0.5 (t, ¹J_{BF} = 29 Hz). ¹³C{¹H} NMR (101.6 MHz, CDCl₃): δ 149.0, 141.7, 140.0, 139.1, 131.1, 129.6, 129.4, 125.4, 123.2, 21.34, 21.32. ¹⁹F NMR (376.1 MHz, CDCl₃): δ -145.0 (q, ¹J_{FB} = 30 Hz). FT-IR (ATR, cm⁻¹): 3033, 2916, 2858, 1909, 1605, 1506, 1504, 1414, 1377, 1350, 1317, 1302. UV-vis (toluene): λ_{max} = 317 nm (ε = 21900 M⁻¹ cm⁻¹), 532 nm (ε = 20200 M⁻¹ cm⁻¹). ESI-HRMS (+ve mode): calculated for [C₂₂H₂₁BF₂N₄]⁺: 390.1827, found 390.1841, difference: +3.6 ppm.

Dialkynylborane Complex 10a: Under N₂, phenylacetylene (0.13 mL, 1.1 mmol) was dissolved in dry THF (5 mL) in a greaseless Schlenk flask, cooled to -78 °C, and stirred for 30 min. *n*-BuLi (1.6 M, 0.45 mL, 1.1 mmol) was added dropwise over 5 min and the solution was stirred for 1 h. The solution was then brought to room temperature, stirred for 30 min, and added dropwise to a second greaseless Schlenk flask containing BF₂ complex **9** (0.20 g, 0.50 mmol)

dissolved in THF (10 mL). The solution was stirred for 2 h at room temperature and gradually changed color from deep purple to red/orange. The solution was then quenched with deionized H₂O (7 mL), extracted with Et₂O that was subsequently washed with deionized H₂O (3 × 50 mL), dried over MgSO₄, gravity filtered and concentrated *in vacuo*. The resulting residue was purified by flash chromatography (2:1 hexanes:CH₂Cl₂, silica gel) to afford complex **10a** as a red/orange microcrystalline solid after solvent removal *in vacuo*. Yield = 0.10 g (35%). M.p. 153–155 °C. ¹H NMR (599.5 MHz, CDCl₃): δ 8.02–7.99 (m, 2H, Aryl CH), 7.91–7.88 (m, 4H, Aryl CH), 7.28–7.19 (m, 16H, Aryl CH), 2.43 (s, 3H, CH₃), 2.42 (s, 6H, CH₃). ¹¹B NMR (128.3 MHz, CDCl₃): δ –11.8 (s). ¹³C{¹H} NMR (101.6 MHz, CDCl₃): δ 151.7, 143.3, 139.4, 138.7, 131.5, 131.3, 129.3, 128.5, 127.9, 127.5, 125.5, 125.2, 124.4, 99.9, 77.2, 21.38, 21.35. FT-IR (ATR, cm⁻¹): 3030, 2952, 2920, 2854, 2367, 2341, 2187, 1598, 1491, 1489, 1442, 1350, 1280. UV-vis (toluene): λ_{max} = 320 nm (ε = 25700 M⁻¹ cm⁻¹), 521 nm (ε = 12000 M⁻¹ cm⁻¹). ESI-HRMS (+ve mode): calculated for [C₃₈H₃₁BN₄]⁺: 554.2642, found 554.2651, difference: +1.6 ppm.

Dialkynylborane Complex 10b: Under N₂, 4-methoxyphenylacetylene (0.22 g, 1.7 mmol) was dissolved in dry THF (5 mL) in a greaseless Schlenk flask, cooled to –78 °C, and stirred for 30 min. *n*-BuLi (1.6 M, 0.68 mL, 1.7 mmol) was added dropwise over 5 min and the solution was stirred for 1 h. The solution was then brought to room temperature and slowly changed from clear yellow to an opaque coffee-brown color. The solution was stirred for 30 min, added dropwise to a second greaseless Schlenk flask containing BF₂ complex **9** (0.30 g, 0.8 mmol) dissolved in THF (10 mL) and stirred for an additional 2 h. The resulting solution gradually changed from deep purple to red and finally brown. The solution was then quenched with deionized H₂O (7 mL), extracted with Et₂O that was subsequently washed with deionized H₂O (3 × 50 mL), dried over MgSO₄, gravity filtered and concentrated *in vacuo*. The resulting residue

was purified by flash chromatography (toluene, silica gel) to afford complex **10b** as a red/brown microcrystalline solid after solvent removal *in vacuo*. Yield = 0.08 g (17%). M.p. 152–154 °C. ¹H NMR (399.8 MHz, CDCl₃): δ 8.02–7.98 (m, 2H, Aryl CH), 7.91–7.86 (m, 4H, Aryl CH), 7.28–7.26 (m, 2H, Aryl CH), 7.23–7.21(m, 4H, Aryl CH), 7.17–7.15 (m, 4H, Aryl CH), 6.73–6.71 (m, 4H, Aryl CH), 3.76 (s, 6H, OCH₃), 2.42 (s, 3H, CH₃), 2.41 (s, 6H, CH₃). ¹¹B NMR (128.3 MHz, CDCl₃): δ –11.8 (s). ¹³C{¹H} NMR (101.6 MHz, CDCl₃): δ 159.0, 151.7, 143.3, 139.2, 138.7, 132.9, 131.4, 129.2, 128.4, 125.6, 125.2, 116.8, 113.5, 99.7, 77.2, 55.2, 21.38, 21.35. FT-IR (ATR, cm⁻¹): 3038, 2956, 2926, 2854, 2189, 1605, 1508, 1464, 1441, 1355, 1282. UV-vis (toluene): λ_{max} = 317 nm (ε = 23400 M⁻¹ cm⁻¹), 519 nm (ε = 12500 M⁻¹ cm⁻¹). ESI-HRMS (+ve mode): calculated for [C₄₀H₃₅BN₄O₂]⁺: 614.2853, found 614.2879, difference: +4.2 ppm.

Dialkynylborane Complex 10c: Under N₂, 4-trifluoromethylphenylacetylene (0.28 mL, 1.7 mmol) was dissolved in dry THF (5 mL) in a greaseless Schlenk flask, cooled to –78 °C, and stirred for 30 min. *n*-BuLi (1.6 M, 0.68 mL, 1.7 mmol) was added dropwise over 5 min and the solution was stirred for 1 h. While stirring, the solution changed from clear yellow to cloudy white. The solution was held at –78 °C and then added dropwise to a second greaseless Schlenk flask containing BF₂ complex **9** (0.3 g, 0.8 mmol) dissolved in THF (10 mL) at –78 °C. The deep purple solution slowly turned orange/brown as the solution was brought from –78 °C to room temperature and stirred for 2 h. The solution was then quenched with deionized H₂O (7 mL), extracted with Et₂O that was subsequently washed with deionized H₂O (3 × 50 mL), dried over MgSO₄, gravity filtered and concentrated *in vacuo*. The resulting residue was purified by flash chromatography (silica gel). The column was first flushed with hexanes (50 mL) to remove impurities, followed by toluene (50 mL) to afford complex **10c** as a purple/brown

microcrystalline solid after solvent removal *in vacuo*. Yield = 0.09 g (17%). M.p. 155–157 °C. ^1H NMR (399.8 MHz, CDCl_3): δ 8.02–7.98 (m, 2H, Aryl CH), 7.87–7.83 (m, 4H, Aryl CH), 7.48–7.44 (m, 4H, Aryl CH), 7.32–7.24 (m, 10H, Aryl CH), 2.43 (m, 9H, CH_3). ^{11}B NMR (128.3 MHz, CDCl_3): δ –12.0 (s). $^{13}\text{C}\{^1\text{H}\}$ NMR (101.6 MHz, CDCl_3): δ 152.1, 143.1, 139.7, 139.1, 131.7, 130.9, 129.5, 129.4, 129.2, 128.6, 127.9, 125.5, 125.2, 124.9 (q, $^1J_{\text{CF}} = 16$ Hz), 122.6, 98.6, 77.2, 21.38, 21.36. ^{19}F NMR (376.1 MHz, CDCl_3) δ –62.8 (s). FT-IR (ATR, cm^{-1}): 3043, 2976, 2926, 2872, 2188, 1926, 1615, 1506, 1405, 1320, 1278, 1263. UV-vis (toluene): $\lambda_{\text{max}} = 317$ nm ($\epsilon = 24900 \text{ M}^{-1} \text{ cm}^{-1}$), 521 nm ($\epsilon = 13700 \text{ M}^{-1} \text{ cm}^{-1}$). ESI-HRMS (+ve mode): calculated for $[\text{C}_{40}\text{H}_{29}\text{BF}_6\text{N}_4]^+$: 690.2389, found 690.2403, difference: +2.0 ppm.

Dialkynylborane Complex 10d: Under N_2 , ethynylferrocene (0.36 g, 1.7 mmol) was dissolved in dry THF (5 mL) in a greaseless Schlenk flask, cooled to -78 °C and stirred for 30 min. *n*-BuLi (0.68 mL, 1.7 mmol) was added dropwise over 5 min and the solution was stirred for 1 h. The solution was then brought to room temperature and stirred for 30 min before it was added dropwise to a second greaseless Schlenk flask containing BF_2 complex **9** (0.31 g, 0.79 mmol) dissolved in THF (10 mL). The solution was then stirred at room temperature for 2 h and quenched with deionized H_2O (7 mL), the organics were extracted with Et_2O that was subsequently washed with deionized H_2O (3×50 mL), dried over MgSO_4 , gravity filtered and concentrated *in vacuo*. The resulting residue was purified by flash chromatography (silica gel). The column was first flushed with hexanes (150 mL) to remove impurities, followed by toluene (50 mL) to afford the resulting complex **10d** as a red/orange microcrystalline solid after solvent removal *in vacuo*. Yield = 0.12 g (19%). M.p. 202–204 °C. ^1H NMR (399.8 MHz, CDCl_3): δ 8.06–8.02 (m, 2H, Aryl CH), 7.91–7.86 (m, 4H, Aryl CH), 7.30–7.26 (m, 6H, Aryl CH), 4.22 (t, 4H, $J_{\text{HH}} = 4$ Hz, Aryl CH), 4.05 (t, 4H, $J_{\text{HH}} = 4$ Hz, Aryl CH), 3.92 (s, 10H, Aryl CH), 2.42 (s,

9H, CH₃). ¹¹B NMR (128.3 MHz, CDCl₃): δ -11.8 (s). ¹³C{¹H} NMR (101.6 MHz, CDCl₃): δ 151.8, 143.4, 139.2, 138.7, 131.4, 129.3, 128.4, 125.6, 125.1, 98.2, 77.2, 71.2, 69.6, 68.0, 66.6, 21.39, 21.36. FT-IR (ATR, cm⁻¹): 3093, 3037, 2957, 2923, 2854, 2358, 2189, 1739, 1605, 1506, 1456, 1353, 1282, 1263. UV-vis (toluene): λ_{max} = 317 nm (ε = 13400 M⁻¹ cm⁻¹), 517 nm (ε = 6800 M⁻¹ cm⁻¹). ESI-HRMS (+ve mode): calculated for [C₄₆H₃₉BF₂N₄]⁺: 770.1967, found 770.1977, difference: +1.3 ppm.

Dialkynylborane Complex 10e: Under N₂, trimethylsilylacetylene (0.27 mL, 1.9 mmol) was dissolved in dry THF (5 mL) in a greaseless Schlenk flask, cooled to -78 °C and stirred for 30 min. *n*-BuLi (0.79 mL, 1.9 mmol) was added dropwise over 5 min and the solution was stirred for 1h. The solution was held at -78 °C and then added dropwise to a second greaseless Schlenk flask containing BF₂ complex **9** (0.35 g, 0.90 mmol) dissolved in THF (10 mL) at -78 °C. The deep purple solution slowly turned red/orange as the solution was warmed from -78 °C to room temperature and stirred for 3 h. The solution was then quenched with deionized H₂O (7 mL), the organics were extracted with Et₂O that was subsequently washed with deionized H₂O (3 × 50 mL), dried over MgSO₄, gravity filtered and concentrated *in vacuo*. The resulting residue was purified by flash chromatography (toluene, silica gel) to afford the resulting complex **10e** as a purple/brown greasy solid after solvent removal *in vacuo*. Yield = 0.15 g (31%). ¹H NMR (399.8 MHz, CDCl₃): δ 7.94–7.90 (m, 2H, Aryl CH), 7.78–7.74 (m, 4H, Aryl CH), 7.27–7.22 (m, 2H, Aryl CH), 7.19–7.15 (m, 4H, Aryl CH), 2.41 (s, 3H, CH₃), 2.38 (s, 6H, CH₃), -0.05 (s, 18H, CH₃). ¹¹B NMR (128.3 MHz, CDCl₃): δ -13.2 (s). ¹³C{¹H} NMR (101.6 MHz, CDCl₃): δ 152.6, 142.8, 139.2, 138.8, 131.0, 129.1, 128.3, 125.7, 125.3, 106.8, 77.2, 21.4, 21.3, -0.3. FT-IR (ATR, cm⁻¹): 3035, 2957, 2923, 2897, 2857, 2132, 1605, 1505, 1351, 1260, 1247, 1209. UV-

vis (toluene): $\lambda_{\max} = 317 \text{ nm}$ ($\epsilon = 25100 \text{ M}^{-1} \text{ cm}^{-1}$), 515 nm ($\epsilon = 14200 \text{ M}^{-1} \text{ cm}^{-1}$). ESI-HRMS (+ve mode): calculated for $[\text{C}_{32}\text{H}_{39}\text{BN}_4\text{Si}_2]^+$: 546.2806, found 546.2770, difference: -6.6 ppm .

Radical anion $10\mathbf{a}^{\cdot-}$: In a N_2 filled glovebox, complex **10a** (0.29 g, 0.51 mmol) was dissolved in toluene (15 mL) and stirred for 15 min. Separately, bis(cyclopentadienyl)cobalt (II) (0.10 g, 0.51 mmol) was dissolved in toluene (6 mL) and stirred for 15 min. The solution was then added dropwise to the solution of **10a** and stirred for 4 h. The resulting brown/green suspension was then vacuum filtered and the solid was washed with toluene (5 mL) followed by pentane (10 mL) to afford **10a $^{\cdot-}$** as a green powder. Yield = 0.31 g (81%). M.p. 200–202 °C. FT-IR (ATR, cm^{-1}): 3098, 3015, 2919, 2858, 1500, 1485, 1415, 1327, 1278, 1260. UV-vis (CH_3CN): $\lambda_{\max} = 260 \text{ nm}$ ($\epsilon = 70400 \text{ M}^{-1} \text{ cm}^{-1}$), 308 nm ($\epsilon = 23300 \text{ M}^{-1} \text{ cm}^{-1}$), 465 nm ($\epsilon = 11900 \text{ M}^{-1} \text{ cm}^{-1}$), 787 nm ($\epsilon = 3800 \text{ M}^{-1} \text{ cm}^{-1}$), 826 nm ($\epsilon = 3450 \text{ M}^{-1} \text{ cm}^{-1}$). ESI-HRMS (–ve mode): calculated for $[\text{C}_{38}\text{H}_{31}\text{BN}_4]^-$: 554.2647, found 554.2642, difference: -0.9 ppm .

Radical anion $10\mathbf{d}^{\cdot-}$: In an N_2 filled glovebox, complex **10d** (0.18 g, 0.23 mmol) was dissolved in toluene (15 mL) and stirred for 15 min. Separately, bis(pentamethylcyclopentadienyl)cobalt(II) (0.075 g, 0.23 mmol) was dissolved in toluene (6 mL) and stirred for 15 min. This solution was then added dropwise to the solution of **10d** and stirred for 4 h. The resulting emerald green suspension was then vacuum filtered and the solid was washed with toluene (5 mL) followed by pentane (10 mL) to afford **10d $^{\cdot-}$** as a microcrystalline green powder. Yield = 0.27 g (89%). M.p. 171–173 °C (decomp.). FT-IR (ATR, cm^{-1}): 3096, 3078, 3021, 2991, 2958, 2916, 2853, 2156, 1716, 1602, 1501, 1374, 1334. UV-vis (CH_3CN): $\lambda_{\max} = 294 \text{ nm}$ ($\epsilon = 43450 \text{ M}^{-1} \text{ cm}^{-1}$), 470 nm ($\epsilon = 9600 \text{ M}^{-1} \text{ cm}^{-1}$), 767 nm ($\epsilon = 2700 \text{ M}^{-1} \text{ cm}^{-1}$), 833 nm ($\epsilon = 2350 \text{ M}^{-1} \text{ cm}^{-1}$). ESI-HRMS (–ve mode): calculated for $[\text{C}_{46}\text{H}_{39}\text{BFe}_2\text{N}_4]^-$: 770.1972, found 770.1967, difference: -0.6 ppm .

Dialkynylborane Complex 11: In air, complex **10e** (0.41 g, 0.74 mmol) was dissolved in warm MeOH (50 mL). K_2CO_3 (1.5 g, 11 mmol) was added and the solution was stirred at room temperature for 4 h. The solution was then concentrated *in vacuo* and the resulting residue was extracted with Et_2O and deionized H_2O (3×50 mL), dried over $MgSO_4$, gravity filtered and concentrated *in vacuo*. The resulting residue was purified by flash chromatography (1:1 hexanes: CH_2Cl_2 , silica gel) to afford the resulting complex **11** as a purple microcrystalline solid after solvent removal *in vacuo*. Yield = 0.25 g (84%). M.p. 146–148 °C. 1H NMR (399.8 MHz, $CDCl_3$): δ 7.98–7.94 (m, 2H, Aryl CH), 7.77–7.73 (m, 4H, Aryl CH), 7.29–7.25 (m, 2H, Aryl CH), 7.24–7.20 (m, 4H, Aryl CH), 2.41 (s, 3H, CH_3), 2.40 (s, 6H, CH_3), 2.22 (s, 2H, Alkyne CH). ^{11}B NMR (128.3 MHz, $CDCl_3$): δ –13.3 (s). $^{13}C\{^1H\}$ NMR (101.6 MHz, $CDCl_3$): δ 151.6, 143.0, 139.6, 139.0, 130.9, 129.3, 128.6, 125.5, 125.1, 88.1, 77.2, 21.4, 21.3. FT-IR (ATR, cm^{-1}): 3281, 3031, 2921, 2060, 1606, 1506, 1353, 1281, 1264, 1177. UV-vis (toluene): λ_{max} = 317 nm (ϵ = 24200 $M^{-1} cm^{-1}$), 524 nm (ϵ = 14400 $M^{-1} cm^{-1}$). ESI-HRMS (+ve mode): calculated for $[C_{26}H_{23}BN_4]^+$: 402.2016, found 402.2017, difference: +0.2 ppm.

Bis(triazolyl)borane Complex 12: Under N_2 , *N,N,N',N'',N''*-pentamethyldiethylenetriamine (3 μ L, 0.02 mmol) and CuI (0.003 g, 0.02 mmol) were dissolved in dry THF (3 mL) and stirred for 30 min. The solution gradually changed from clear to pale yellow. Benzyl azide (58 μ L, 0.50 mmol) was added dropwise followed by complex **11** (0.062 g, 0.2 mmol). The resulting purple solution was diluted with THF (7 mL) and stirred at 45 °C for 18 h. The solution was then cooled to room temperature, gravity filtered and the supernatant concentrated *in vacuo*. The resulting residue was purified by flash chromatography (CH_2Cl_2 , silica gel) to afford complex **12** as a purple microcrystalline solid after solvent removal *in vacuo*. Yield = 0.050 g (38%). M.p. 169–171 °C. 1H NMR (399.8 MHz, $CDCl_3$): δ 8.06–8.03 (m, 2H, Aryl CH), 7.37–7.35 (m, 6H,

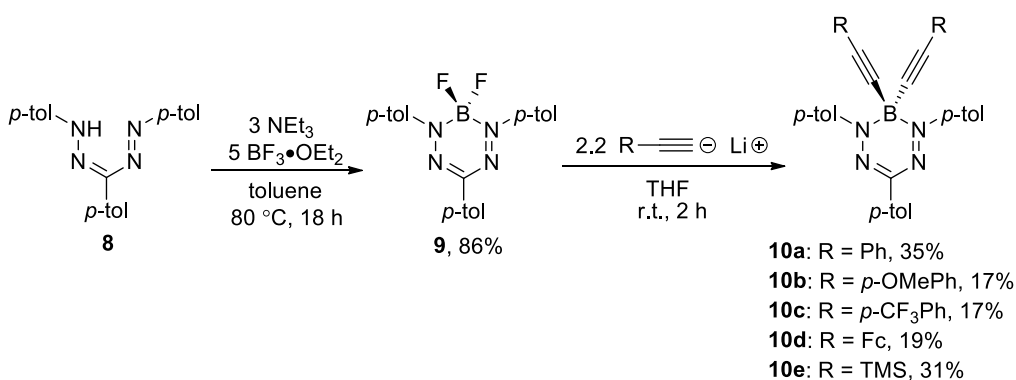
Aryl CH), 7.31 (d, 2H, $J_{HH} = 8$ Hz, Aryl CH), 7.26–7.24 (m, 6H, Aryl CH and triazolyl CH), 7.08–7.06 (m, 4H, Aryl CH), 6.97–6.94 (m, 4H, Aryl CH), 5.35 (s, 4H, Benzyl CH), 2.44 (s, 3H, CH₃), 2.32 (s, 6H, CH₃). ¹¹B NMR (128.3 MHz, CDCl₃): δ –6.0 (s). ¹³C{¹H} NMR (101.6 MHz, CDCl₃): δ 153.8, 143.2, 139.4, 139.2, 136.4, 135.6, 130.7, 129.4, 129.2, 129.1, 128.4, 125.7, 125.5, 124.5, 77.2, 52.1, 21.4, 21.2. FT-IR (ATR, cm⁻¹): 3034, 2926, 2855, 1604, 1505, 1355, 1282, 1262, 1211, 954, 821. UV-vis (toluene): λ_{max} = 295 nm (ε = 29750 M⁻¹ cm⁻¹), 532 nm (ε = 13100 M⁻¹ cm⁻¹). ESI-HRMS (+ve mode): calculated for [C₄₀H₃₇BN₁₀]⁺: 668.3296, found 668.3314, difference: +2.7 ppm.

RESULTS AND DISCUSSION

Synthesis and X-ray Crystallography

Formazan **8** was synthesized according to a published procedure⁷⁰ and was converted to the corresponding BF₂ formazanate **9** in 86% yield by heating an excess of BF₃•OEt₂ and NEt₃ at 80 °C in toluene under anhydrous conditions for 18 h (Scheme 1). This transformation was accompanied by a loss of the NH resonance at 15.42 ppm in the ¹H NMR spectrum of formazan **8** and the appearance of a triplet at –0.5 ppm (¹J_{BF} = 29 Hz) in the ¹¹B NMR spectrum and a quartet at –145.0 ppm (¹J_{FB} = 30 Hz) in the ¹⁹F NMR spectrum of **9** (Figures S1–S3). BF₂ complex **9** was subsequently converted to dialkynylborane complexes **10a–10e** by treatment with a slight excess of the lithium salts of a series of substituted alkynes according to Scheme 1. The yields of these reactions, which were generally lower than those observed for the synthesis of related BODIPYs,⁷¹ reflected the steric congestion at boron imposed by the *N*-aryl substituents of the formazanate ligand framework and ranged from 17–35%. After workup, the mass balance for these reactions was made up of trace amounts of the parent formazan, which was regenerated

during the reaction, and other highly colored decomposition products that we have been unable to identify. The degree of decomposition increased when alkynyl lithium reagents were replaced with the corresponding Grignards and the synthetic pathway employed was not compatible with 3-cyanoformazanate complexes due to the apparent reactivity between the carbanions employed and the cyano substituents of the ligand backbone. Despite these considerations, our synthetic approach takes advantage of the ready accessibility of formazans and circumvents many of the challenges associated with BODIPY synthesis. The NMR spectra collected for complexes **10a–10e** indicated that the *N*-aryl substituents were equivalent on the NMR timescale (Figures S4–S19). Notably, the ^{11}B NMR spectra for these compounds were comprised of broadened singlets that appeared between -11.8 and -13.2 ppm. The intensity of these resonances was diminished compared to the ^{11}B NMR resonance observed for **9** due to the decreased Nuclear Overhauser Effect that resulted from the replacement of a fluorine atom with a substituted alkynyl ligand. FT-IR spectroscopy and mass spectrometry data corroborated the proposed structures of complexes **10a–10e**.



Scheme 1. Synthesis of dialkynylborane complexes **10a–10e**.

To gain further insight into the structure and bonding associated with complexes **10a–10e** and **9**, we employed single-crystal X-ray diffraction measurements (Figure 1, Table 1, Table S1).

The solid-state structures of complexes **9**, **10a**, and **10d** provide an indication that the π -systems of the formazanate ligand backbones are highly delocalized, with N-N [1.3028(7)–1.316(3) Å] and C-N [1.3385(8)–1.352(2) Å] bond lengths falling between what would normally be expected for single and double bonds of the same atoms.⁷² The most significant difference in the structures of **10a** and **10d** when compared to that of the BF₂ complex **9** is the position of the boron atom relative to the plane defined by the four nitrogen atoms of the formazanate backbone (N₄: N1, N2, N3, N4) and the related twisting of the *N*-aryl substituents relative to the same plane. The solid-state structure of **9** is highly planar and consistent with most other BF₂ formazanates,⁶⁹ with the boron atom sitting 0.094 Å above the N₄ plane and average angles between the plane defined by the *N*-aryl substituent and the N₄ plane of 6.50°. In contrast, the structure adopted by **10a** significantly deviates from planarity. The boron atom is displaced from the N₄ plane by 0.713 Å and the average angle between the N₄ plane and the *N*-aryl substituents is 57.76°. These metrics are further exaggerated in the solid-structure of **10d**, with corresponding values of 0.755 Å and 67.40°. We postulate that the observed conformations are adopted as a result of optimized solid-state packing rather than steric effects implicating the boron- and nitrogen-bound substituents. Similar conformations have been occasionally observed for BF₂ formazanates indicating that there is a relatively small energetic penalty associated with deviations from planarity.⁵⁵ Furthermore, low temperature ¹H NMR spectra collected for complex **10d** did not provide evidence for the presence of inequivalent ferrocene environments that would be expected if a similar conformation existed in solution (Figure S20).

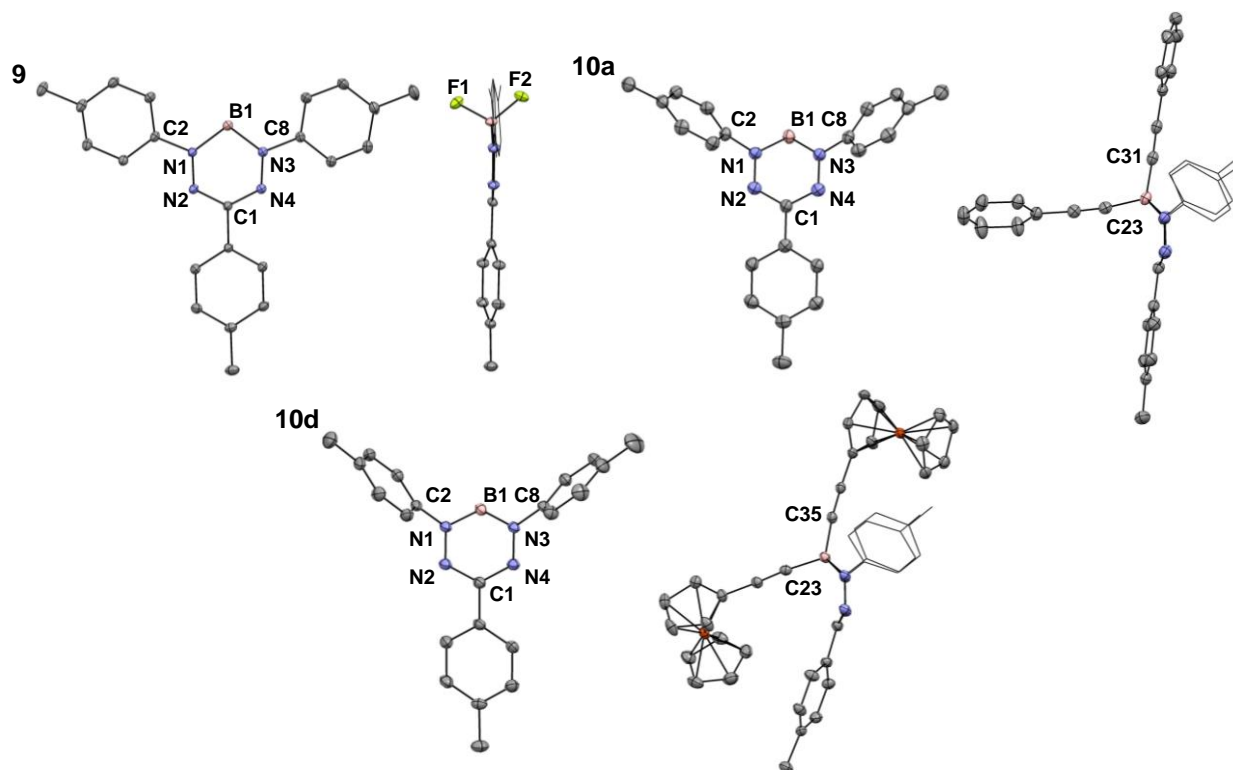


Figure 1. Top and side views of the solid-state structures of compounds **9**, **10a**, and **10d**. Anisotropic displacement ellipsoids are shown at the 50% probability level. Hydrogen atoms and alkyne substituents (top view) have been omitted and *N*-aryl substituents (side view) have been displayed in wireframe format for clarity.

Table 1. Selected bond lengths (Å), bond angles (°), and structural metrics extracted from the solid-state structures of compounds **9**, **10a**, and **10d**.

	9	10a	10d
B1-N1	1.566(1)	1.575(4)	1.576(3)
B1-N3	1.5604(9)	1.573(3)	1.581(3)
N1-N2	1.3037(7)	1.312(3)	1.313(2)
N3-N4	1.3028(7)	1.316(3)	1.308(2)
C1-N2	1.3417(8)	1.346(3)	1.343(2)
C1-N4	1.3385(8)	1.344(3)	1.352(2)
N1-B1-N3	106.10(5)	97.49(2)	96.10(1)
N2-N1-B1	124.66(5)	118.44(2)	117.48(1)
N4-N3-B1	124.17(5)	118.16(2)	118.13(1)
N2-C1-N4	126.46(5)	121.67(2)	120.96(2)
Dihedral Angles ^a	4.51, 8.48	54.92, 60.60	66.87, 67.92
Boron Displacement ^b	0.094	0.713	0.755

^aThe angle between the planes defined by the *N*-aryl substituents and the N₄ plane of the formazanate ligand backbone. ^bThe distance between B1 and the N₄ plane of the formazanate ligand backbone.

Electronic Properties

The structural metrics highlighted above have implications on the UV-vis absorption spectra of compounds **9** and **10a–10d** (Figure 2 and Table 2). The parent BF₂ complex **9** has a low-energy absorption maximum (λ_{max}) of 532 nm with a molar absorptivity (ϵ) of 20200 M⁻¹ cm⁻¹. This transition has previously been demonstrated to be highly dependent on the nature of the *N*-aryl substituents of the formazanate ligand and assigned as a $\pi \rightarrow \pi^*$ transition involving primarily the highest occupied molecular orbital (HOMO) and lowest unoccupied molecular orbital (LUMO) orbitals.⁵⁵ Relative to the spectrum obtained for **9**, this band was blue-shifted and less intense in the spectra obtained for **10a–10d** with λ_{max} values ranging from 517 to 521 nm and ϵ values ranging from 6800 to 13700 M⁻¹ cm⁻¹. The absorption maxima associated with the $\pi \rightarrow \pi^*$ transition for complexes **10a–10d** appeared at energies that were similar to *E*-BODIPYs⁷³ and were not solvatochromic. They also showed little to no dependence on the nature of the alkynyl substituent as these substituents lie in a plane that is orthogonal to the formazanate ligand backbone. Complexes **9** and **10a–10d** were essentially non-emissive in solution and the solid state with photoluminescence quantum yields less than 1%.

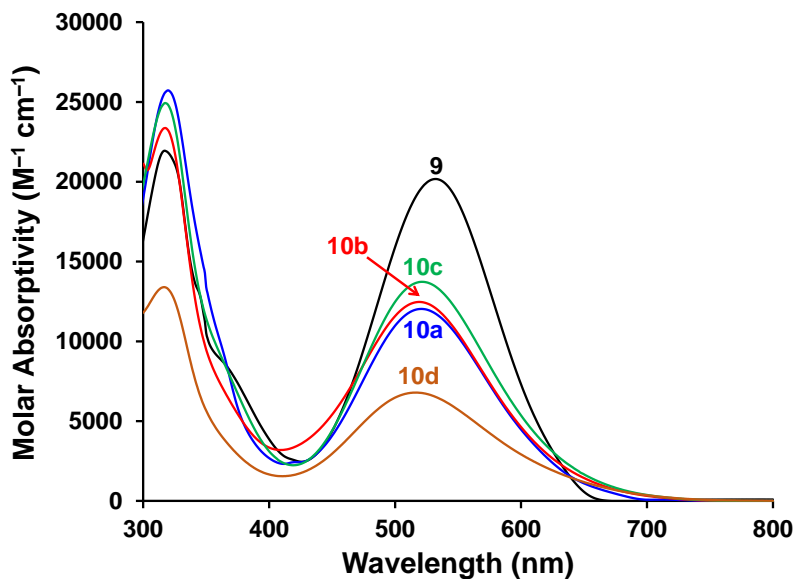
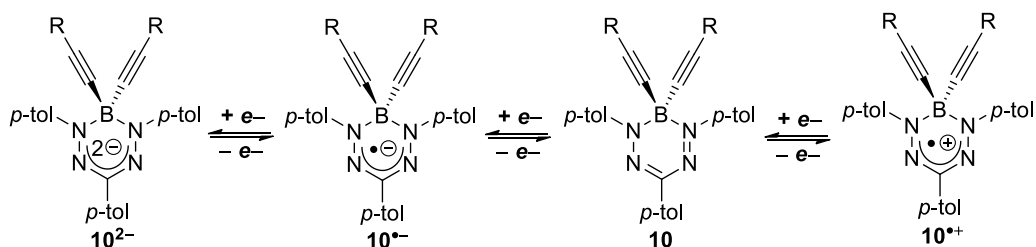


Figure 2. UV-vis absorption spectra of compounds **9** and **10a–10d** recorded for 10 μ M toluene solutions.

A differentiating feature between borane complexes of formazanates and complexes of most other chelating *N*-donor ligands is their redox activity. In order to probe the redox activity of complexes **9** and **10a–10d**, solution phase cyclic voltammetry (CV) was employed (Figure 3, Table 2). Complex **9** was reversibly oxidized to its radical cation $\mathbf{9}^{\bullet+}$ at $E_{\text{ox}1} = 1.03$ V relative to the ferrocene/ferrocenium redox couple. Consistent with other BF_2 formazanates, it also underwent stepwise one-electron reductions to the corresponding radical anion $\mathbf{9}^{\bullet-}$ and dianion $\mathbf{9}^{2-}$ at potentials of $E_{\text{red}1} = -1.04$ V and $E_{\text{red}2} = -1.99$ V.⁶⁹ The second reduction was irreversible under our experimental conditions, likely due to a chemical reaction between the extremely electron-rich dianion and a component of the analyte solution that regenerates the radical anion. The electrochemical properties of **10a–10d**, which implicated the species highlighted in Scheme 2, were qualitatively similar. In the case of compounds **10b–d**, the first reduction was not formally reversible when the full electrochemical window of the solvent was scanned. However, the first reduction wave became reversible when a narrower potential window that excluded the

second reduction wave was examined (Figure S21). In all cases the dialkynylborane complexes were easier to oxidize and more difficult to reduce than the corresponding BF_2 complex due to the greater electron-donating character of alkynyl substituents compared to the fluorine atoms. Comparison of the CVs of **10a–10c** provides an indication of the effect of the substituted alkyne substituents on the electronic structure of the compounds. Complex **10a** ($\text{R} = \text{Ph}$) was reduced at potentials of $E_{\text{red1}} = -1.18 \text{ V}$ and $E_{\text{red2}} = -2.03 \text{ V}$. The introduction of electron-donating *p*-OMePh substituents in **10b** rendered the complex more difficult to reduce as indicated by the negatively-shifted reduction potentials $E_{\text{red1}} = -1.21 \text{ V}$ and $E_{\text{red2}} = -2.12 \text{ V}$. The *p*- CF_3Ph substituents of **9c** had the opposite effect, shifting the reduction potentials to more positive values of $E_{\text{red1}} = -1.14 \text{ V}$ and $E_{\text{red2}} = -2.01 \text{ V}$. The potentials corresponding to the oxidation of compounds **10a–10c** followed a similar trend, although direct comparison was complicated by the irreversibility of the oxidation wave corresponding to complex **10b** ($\text{R} = p\text{-OMePh}$). In addition to the electrochemical features discussed above, complex **10d** ($\text{R} = \text{Fc}$) gave rise to a reversible wave, that corresponded to twice the current of the first reduction wave, centered at a potential $E_{\text{Fc}/\text{Fc}^+} = 0.03 \text{ V}$. This observation is consistent with two coincident (or near coincident) one-electron processes corresponding to the oxidation of two electron-rich ferrocene groups.



Scheme 2. Electrochemically relevant forms of dialkynylborane formazanate complexes **10**.

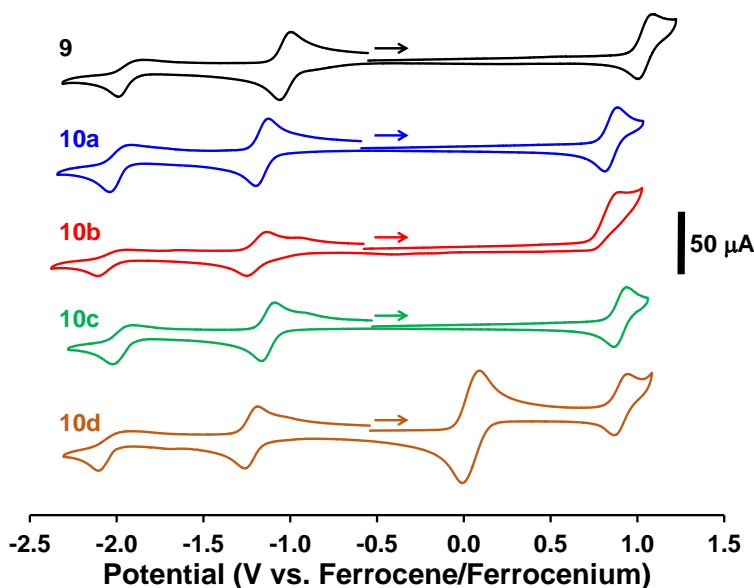


Figure 3. CVs of compounds **9** and **10a–10d** recorded in dry, degassed CH_2Cl_2 containing ~ 1 mM analyte and 0.1 M $[\text{nBu}_4\text{N}][\text{PF}_6]$ as a supporting electrolyte at a scan rate of 250 mV s^{-1} . The arrows indicate the scan direction.

Table 2. Solution-state characterization data for compounds **9** and **10a–10d**.

Compound	λ_{max} (nm) ^a	ϵ ($\text{M}^{-1} \text{cm}^{-1}$) ^a	E_{red2} (V) ^b	E_{red1} (V) ^b	$E_{\text{Fc/Fc}^+}$ (V) ^b	E_{ox1} (V) ^b
9	532	20200	-1.99 ^c	-1.04	-	1.03
10a	521	12000	-2.03 ^c	-1.18	-	0.83
10b	519	12500	-2.12 ^c	-1.21	-	0.86 ^d
10c	521	13700	-2.01 ^c	-1.14	-	0.89
10d	517	6800	-2.09 ^c	-1.21	0.03	0.89

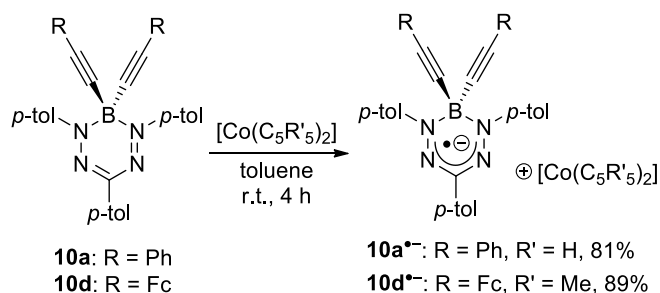
^aRecorded for 10 μM toluene solutions. ^bCVs were recorded for dry, degassed CH_2Cl_2 solutions containing ~ 1 mM analyte and 0.1 M $[\text{nBu}_4\text{N}][\text{PF}_6]$ as a supporting electrolyte at a scan rate of 250 mV s^{-1} . Potentials are reported relative to the ferrocene/ferrocenium redox couple.

^cIrreversible peak. Potential at maximum cathodic current reported. ^dIrreversible peak. Potential at maximum anodic current reported.

Reactivity

Given the reversible oxidation and reduction waves observed in the CVs of compounds **10a–10d**, we attempted to access the radical cation and radical anion forms of complexes **10a** and **10d**. However, we were unable to isolate pure oxidation products formed upon treatment of dialkynylborane complexes with a variety of oxidants, including $[(p\text{-BrC}_6\text{H}_4)_3\text{N}][\text{SbCl}_6]$ (magic

blue), NOBF_4 , and WCl_6 . Conversely, radical anions $\mathbf{10a}^{\bullet-}$ and $\mathbf{10d}^{\bullet-}$ that were stable enough to be isolated and characterized were produced when $\mathbf{10a}$ and $\mathbf{10d}$ were treated with $[\text{Co}(\text{C}_5\text{H}_5)_2]$ and $[\text{Co}(\text{C}_5\text{Me}_5)_2]$, respectively (Scheme 3).



Scheme 3. Chemical reduction of complexes $\mathbf{10a}$ and $\mathbf{10d}$.

Conversion of $\mathbf{10a}$ and $\mathbf{10d}$ to their radical anion forms was accompanied by a dramatic color change in the isolated products from red/orange to green. Dilute solutions of $\mathbf{10a}^{\bullet-}$ and $\mathbf{10d}^{\bullet-}$ yielded isotropic electron paramagnetic resonance (EPR) spectra with g -factors of 2.0035 and UV-vis absorption spectra with bands centered at 787 and 826 nm for $\mathbf{10a}^{\bullet-}$ and 767 and 833 nm for $\mathbf{10d}^{\bullet-}$ (Figure 4 and S22). These spectral features were qualitatively similar to other borataverdazyl-type radicals derived from formazanate ligands.^{53,74}

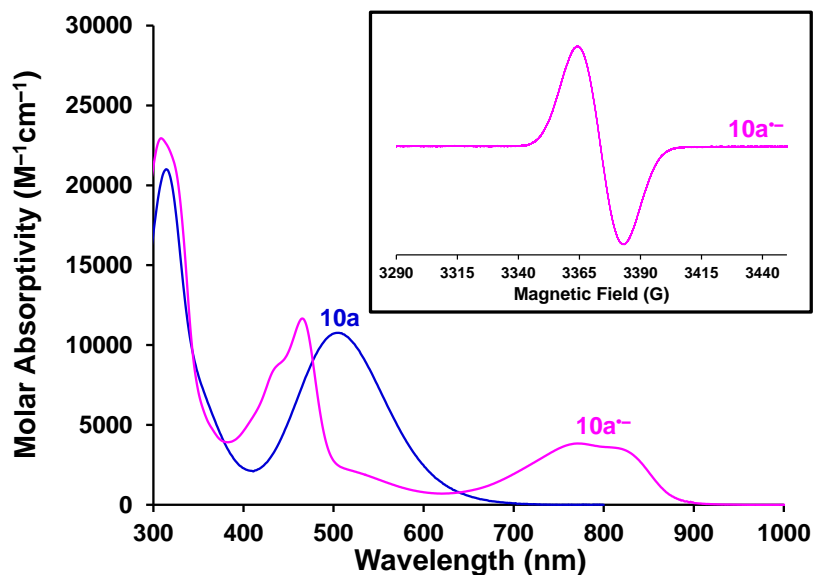
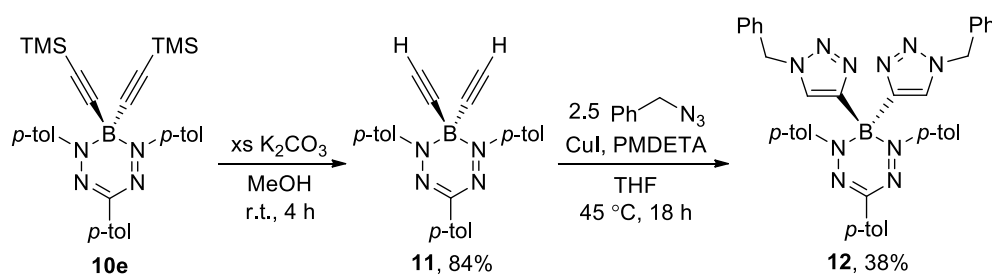


Figure 4. UV-vis absorption spectra of compounds **10a** and **10a⁻** recorded for 10 μ M CH_3CN solutions. The inset shows the EPR spectrum of **10a⁻** recorded in degassed THF ($g = 2.0035$).

Metal-catalyzed cross-coupling reactions have been previously demonstrated for *E*-BODIPYs,⁷⁵ prompting us to conduct a proof-of-concept study to evaluate the suitability of complex **11** to undergo copper-assisted alkyne-azide cycloaddition chemistry as a route to further elaborate the structural diversity associated with dialkynylborane formazante complexes. TMS-protected complex **10e** was deprotected using excess K_2CO_3 to afford alkyne-substituted complex **11** in 84% yield (Scheme 4, Figures S23–S25). This transformation was accompanied by a loss of the 1H NMR resonance at -0.05 ppm associated with the TMS group of **10e** and the appearance of a new resonance at 2.22 ppm due to the presence of the free alkyne substituents of **11**. Bis(triazolyl)borane complex **12** was prepared in 38% yield by combining a mixture of complex **10** and a slight excess of benzyl azide with a catalytic amount of CuI and *N,N,N',N'',N'''*-pentamethyldiethylenetriamine (PMDETA) (Scheme 4, Figures S26–S28). The relatively low yield of this reaction was attributed to the sterically congested environment associated with the boron-bound alkyne substituents in compound **11** and no reaction was observed in the absence of

CuI. The absence of IR absorptions associated with the alkyne substituents of compound **11** (3281 and 2060 cm^{-1}) and benzyl azide (2094 cm^{-1}) in the IR spectrum of **12** (Figure 5) were consistent with the proposed structure, which was confirmed by NMR spectroscopy and mass spectrometry data. The UV-vis absorption spectra of complexes **10e**, **11**, and **12** were qualitatively similar to those of complexes **10a–10d** with λ_{max} values of 515, 524, and 532 nm, respectively (Figure S29).



Scheme 4. Deprotection of complex **10e** and subsequent alkyne-azide cycloaddition chemistry to form complex **12**.

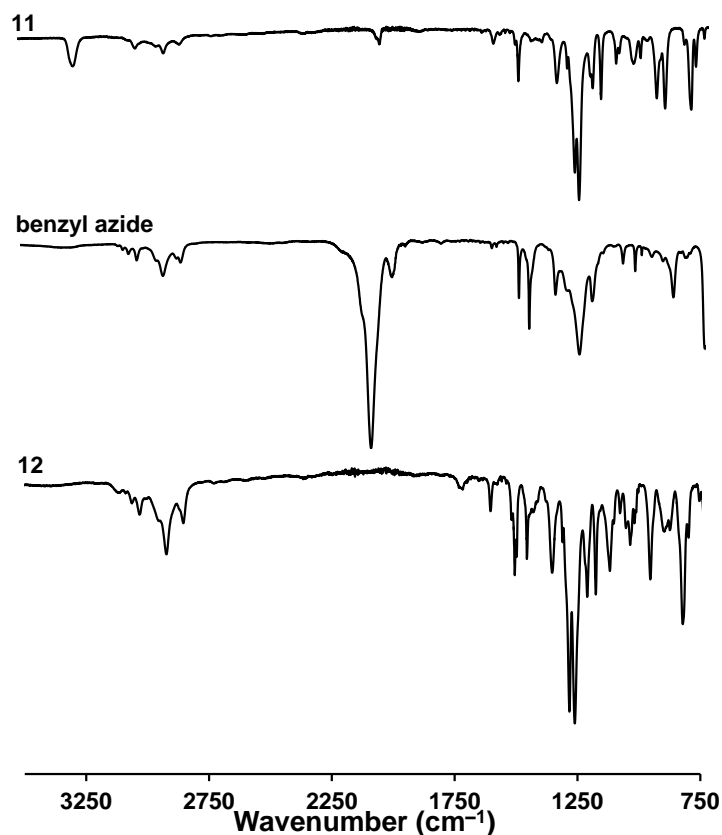


Figure 5. FT-IR spectra of **11**, benzyl azide, and **12**.

CONCLUSIONS

We synthesized a series of novel dialkynylborane complexes, the first based on redox-active formazanate ligands, by reacting a BF_2 formazanate complex with lithium salts of substituted alkynes. The electronic properties of these complexes were studied using UV-vis absorption spectroscopy and cyclic voltammetry. These studies demonstrated that the absorption maxima, and thus HOMO-LUMO gaps, were not dependent on the nature of the alkyne substituents, while similar structural variation affected the potentials at which electrochemical oxidation and reduction occurred. When electron-donating substituents were incorporated, complexes became harder to reduce and easier to oxidize. When electron-withdrawing substituents were introduced, the opposite trend was observed. Chemical reduction of selected

complexes afforded stable radical anions supported by the formazanate ligand backbone and provide a potential handle for the development of redox sensors. Finally, copper-assisted alkyne-azide cycloaddition chemistry was demonstrated to occur at the boron-bound alkynyl substituents of one of our complexes, opening the door to an entirely new mode of reactivity for this class of compounds that should lead to the development of novel functional molecular materials based on dialkynylborane complexes of a variety of *N*-donor ligands in the future.

ASSOCIATED CONTENT

Supporting Information

The supporting information is available free of charge on the ACS Publications website at DOI: #####.

X-ray crystallography methods, data collection and refinement details; ^1H , ^{11}B , $^{13}\text{C}\{^1\text{H}\}$, and ^{19}F NMR spectra for diamagnetic compounds; additional UV-vis absorption and EPR spectra.

AUTHOR INFORMATION

Corresponding Authors

*E-mail: mworkent@uwo.ca; joe.gilroy@uwo.ca. Tel: +1 (519) 661-2111 ext. 86319 (M.S.W.)/
+1 (519) 661-2111 ext. 81561 (J.B.G.).

Author Contributions

The manuscript was written through contributions of all authors. All authors have given approval of the final version of the manuscript.

Notes

The authors declare no competing financial interests.

ACKNOWLEDGEMENTS

This work was supported by the Natural Sciences and Engineering Research Council (NSERC) of Canada (M.S.W.: DG, RGPIN-2017-04637, J.B.G.: DG, RGPIN-2018-04240, R.R.M.: CGS-D Scholarship), the Ontario Ministry of Research and Innovation (J.B.G.: ERA, ER-14-10-147) and the Canadian Foundation for Innovation (J.B.G.: JELF, 33977). The authors thank Dr. Paul Bazylewski and Dr. Giovanni Fanchini for assistance with EPR measurements and access to instrumentation.

REFERENCES

- (1) Loudet, A.; Burgess, K. BODIPY Dyes and Their Derivatives: Syntheses and Spectroscopic Properties. *Chem. Rev.* **2007**, *107*, 4891–4932.
- (2) Frath, D.; Massue, J.; Ulrich, G.; Ziessel, R. Luminescent Materials: Locking π -Conjugated and Heterocyclic Ligands with Boron(III). *Angew. Chem. Int. Ed.* **2014**, *53*, 2290–2310.
- (3) Ni, Y.; Wu, J. Far-Red and Near Infrared BODIPY Dyes: Synthesis and Applications for Fluorescent pH Probes and Bio-imaging. *Org. Biomol. Chem.* **2014**, *12*, 3774–3791.
- (4) Kowada, T.; Maeda, H.; Kikuchi, K. BODIPY-Based Probes for the Fluorescence Imaging of Biomolecules in Living Cells. *Chem. Soc. Rev.* **2015**, *44*, 4953–4972.
- (5) Ulrich, G.; Goze, C.; Guardigli, M.; Roda, A.; Ziessel, R. Pyrromethene Dialkynyl Borane Complexes for "Cascadelle" Energy Transfer and Protein Labeling. *Angew. Chem. Int. Ed.* **2005**, *44*, 3694–3698.
- (6) Harriman, A.; Izzet, G.; Ziessel, R. Rapid Energy Transfer in Cascade-Type BODIPY Dyes. *J. Am. Chem. Soc.* **2006**, *128*, 10868–10875.

- (7) Rachford, A. A.; Ziessel, R.; Bura, T.; Retailleau, P.; Castellano, F. N. Boron Dipyromethene (BODIPY) Phosphorescence Revealed in $[\text{Ir}(\text{ppy})_2(\text{bpy}-\text{C}\equiv\text{C}-\text{BODIPY})]^+$. *Inorg. Chem.* **2010**, *49*, 3730–3736.
- (8) Suk, J.; Omer, K. M.; Bura, T.; Ziessel, R.; Bard, A. J. Electrochemistry and Electrogenerated Chemiluminescence of Some BODIPY Derivatives. *J. Phys. Chem. C* **2011**, *115*, 15361–15368.
- (9) Lu, J.-s.; Ko, S.-B.; Walters, N. R.; Wang, S. N. Decorating BODIPY with Three- and Four-Coordinate Boron Groups. *Org. Lett.* **2012**, *14*, 5660–5663.
- (10) Berhe, S. A.; Rodriguez, M. T.; Park, E.; Nesterov, V. N.; Pan, H.; Youngblood, W. J. Optoelectronic Tuning of Organoborylazadipyromethenes via Effective Electronegativity at the Metalloid Center. *Inorg. Chem.* **2014**, *53*, 2346–2348.
- (11) Maligaspe, E.; Pundsack, T. J.; Albert, L. M.; Zatsikha, Y. V.; Solntsev, P. V.; Blank, D. A.; Nemykin, V. N. Synthesis and Charge-Transfer Dynamics in a Ferrocene-Containing Organoboryl aza-BODIPY Donor-Acceptor Triad with Boron as the Hub. *Inorg. Chem.* **2015**, *54*, 4167–4174.
- (12) Patalag, L. J.; Jones, P. G.; Werz, D. B. BOIMPYs: Rapid Access to a Family of Red-Emissive Fluorophores and NIR Dyes. *Angew. Chem. Int. Ed.* **2016**, *55*, 13340–13344.
- (13) Maeda, C.; Nagahata, K.; Ema, T. Carbazole-Based BODIPYs with Ethynyl Substituents at the Boron Center: Solid-State Excimer Fluorescence in the VIS/NIR Region. *Org. Biomol. Chem.* **2017**, *15*, 7783–7788.
- (14) Harriman, A.; Mallon, L. J.; Elliot, K. J.; Haefele, A.; Ulrich, G.; Ziessel, R. Length Dependence for Intramolecular Energy Transfer in Three- and Four-Color Donor-Spacer-Acceptor Arrays. *J. Am. Chem. Soc.* **2009**, *131*, 13375–13386.

- (15) Bura, T.; Retailleau, P.; Ziessel, R. Efficient Synthesis of Panchromatic Dyes for Energy Concentration. *Angew. Chem. Int. Ed.* **2010**, *49*, 6659–6663.
- (16) Ziessel, R.; Ulrich, G.; Haefele, A.; Harriman, A. An Artificial Light-Harvesting Array Constructed from Multiple Bodipy Dyes. *J. Am. Chem. Soc.* **2013**, *135*, 11330–11344.
- (17) Roland, T.; Heyer, E.; Liu, L.; Ruff, A.; Ludwigs, S.; Ziessel, R.; Haacke, S. A Detailed Analysis of Multiple Photoreactions in a Light-Harvesting Molecular Triad with Overlapping Spectra by Ultrafast Spectroscopy. *J. Phys. Chem. C* **2014**, *118*, 24290–24301.
- (18) Jagtap, K. K.; Shivran, N.; Mula, S.; Naik, D. B.; Sarkar, S. K.; Mukherjee, T.; Maity, D. K.; Ray, A. K. Change of Boron Substitution Improves the Lasing Performance of BODIPY Dyes: A Mechanistic Rationalisation. *Chem. Eur. J.* **2013**, *19*, 702–707.
- (19) Duran-Sampedro, G.; Esnal, I.; Agarrabeitia, A. R.; Bañuelos Prieto, J.; Cerdán, L.; García-Moreno, I.; Costela, A.; Lopez-Arbeloa, I.; Ortiz, M. J. First Highly Efficient and Photostable *E* and *C* Derivatives of 4,4-Difluoro-4-bora-3a,4a-diaza-*s*-indacene (BODIPY) as Dye Lasers in the Liquid Phase, Thin Films, and Solid-State Rods. *Chem. Eur. J.* **2014**, *20*, 2646–2653.
- (20) Didier, P.; Ulrich, G.; Mély, Y.; Ziessel, R. Improved Push-Pull-Push *E*-BODIPY Fluorophores for Two-Photon Cell-Imaging. *Org. Biomol. Chem.* **2009**, *7*, 3639–3642.
- (21) Poirel, A.; Retailleau, P.; De Nicola, A.; Ziessel, R. Synthesis of Water-Soluble Red-Emitting Thienyl-BODIPYs and Bovine Serum Albumin Labeling. *Chem. Eur. J.* **2014**, *20*, 1252–1257.
- (22) Fan, G.; Lin, Y.-X.; Yang, L.; Gao, F.-P.; Zhao, Y.-X.; Qiao, Z.-Y.; Zhao, Q.; Fan, Y.-S.; Chen, Z.; Wang, H. Co-Self-Assembled Nanoaggregates of BODIPY Amphiphiles for Dual Colour Imaging of Live Cells. *Chem. Commun.* **2015**, *51*, 12447–12450.

- (23) Zhang, J.; Yang, M.; Mazi, W.; Adhikari, K.; Fang, M.; Xie, F.; Valenzano, L.; Tiwari, A.; Luo, F.-T.; Liu, H. Unusual Fluorescent Responses of Morpholine-Functionalized Fluorescent Probes to pH via Manipulation of BODIPY's HOMO and LUMO Energy Orbitals for Intracellular pH Detection. *ACS Sens.* **2016**, *1*, 158–165.
- (24) Filatov, M. A.; Karuthedath, S.; Polestshuk, P. M.; Savoie, H.; Flanagan, K. J.; Sy, C.; Sitte, E.; Telitchko, M.; Laquai, F.; Boyle, R. W.; Senge, M. O. Generation of Triplet Excited States via Photoinduced Electron Transfer in *Meso*-Anthra-BODIPY: Fluorogenic Response toward Singlet Oxygen in Solution and in Vitro. *J. Am. Chem. Soc.* **2017**, *139*, 6282–6285.
- (25) Kumaresan, D.; Thummel, R. P.; Bura, T.; Ulrich, G.; Ziessel, R. Color Tuning in New Metal-Free Organic Sensitizers (BODIPYs) for Dye-Sensitized Solar Cells. *Chem. Eur. J.* **2009**, *15*, 6335–6339.
- (26) Rousseau, T.; Cravino, A.; Bura, T.; Ulrich, G.; Ziessel, R.; Roncali, J. Multi-Donor Molecular Bulk Heterojunction Solar Cells: Improving Conversion Efficiency by Synergistic Dye Combinations. *J. Mater. Chem.* **2009**, *19*, 2298–2300.
- (27) Bura, T.; Leclerc, N.; Fall, S.; Lévêque, P.; Heiser, T.; Ziessel, R. Absorption Tuning of Monosubstituted Triazatruxenes for Bulk Heterojunction Solar Cells. *Org. Lett.* **2011**, *13*, 6030–6033.
- (28) Sutter, A.; Retailleau, P.; Huang, W.-C.; Lin, H.-W.; Ziessel, R. Photovoltaic Performance of Novel Push-Pull-Push Thienyl-BODIPY Dyes in Solution-Processed BHJ-Solar Cells. *New J. Chem.* **2014**, *38*, 1701–1710.

- (29) Nagai, A.; Kokado, K.; Miyake, J.; Chujo, Y. Highly Luminescent Nanoparticles: Self-Assembly of Well-Defined Block Copolymers by π - π Stacked BODIPY Dyes as Only a Driving Force. *Macromolecules* **2009**, *42*, 5446–5452.
- (30) Kaloudi-Chantzea, A.; Karakostas, N.; Raptopoulou, C. P.; Psycharis, V.; Saridakis, E.; Griebel, J.; Hermann, R.; Pistolis, G. Coordination-Driven Self Assembly of a Brilliantly Fluorescent Rhomboid Cavitand Composed of BODIPY-Dye Subunits. *J. Am. Chem. Soc.* **2010**, *132*, 16327–16329.
- (31) Iehl, J.; Nierengarten, J.-F.; Harriman, A.; Bura, T.; Ziessel, R. Artificial Light-Harvesting Arrays: Electronic Energy Migration and Trapping on a Sphere and between Spheres. *J. Am. Chem. Soc.* **2012**, *134*, 988–998.
- (32) Olivier, J.-H.; Barberá, J.; Bahaidarah, E.; Harriman, A.; Ziessel, R. Self-Assembly of Charged BODIPY Dyes To Form Cassettes That Display Intracomplex Electronic Energy Transfer and Accrete into Liquid Crystals. *J. Am. Chem. Soc.* **2012**, *134*, 6100–6103.
- (33) Kaloudi-Chantzea, A.; Karakostas, N.; Pitterl, F.; Raptopoulou, C. P.; Glezos, N.; Pistolis, G. Efficient Supramolecular Synthesis of a Robust Circular Light-Harvesting BODIPY-Dye Based Array. *Chem. Commun.* **2012**, *48*, 12213–12215.
- (34) Mula, S.; Frein, S.; Russo, V.; Ulrich, G.; Ziessel, R.; Barberá, J.; Deschenaux, R. Red and Blue Liquid-Crystalline Borondipyrromethene Dendrimers. *Chem. Mater.* **2015**, *27*, 2332–2342.
- (35) Yang, L.; Fan, G.; Ren, X.; Zhao, L.; Wang, J.; Chen, Z. Aqueous Self-Assembly of a Charged BODIPY Amphiphile via Nucleation-Growth Mechanism. *Phys. Chem. Chem. Phys.* **2015**, *17*, 9167–9172.

- (36) Karakostas, N.; Mavridis, I. M.; Seintis, K.; Fakis, M.; Koini, E. N.; Petsalakis, I. D.; Pistolis, G. Highly Efficient and Unidirectional Energy Transfer within a Tightly Self-Assembled Host-Guest Multichromophoric Array. *Chem. Commun.* **2014**, *50*, 1362–1365.
- (37) Kaloudi-Chantzea, A.; Martinou, E.; Seintis, K.; Karakostas, N.; Giastas, P.; Pitterl, F.; Oberacher, H.; Fakis, M.; Pistolis, G. Formation of a Highly-Ordered Rigid Multichromophoric 3D Supramolecular Network by Combining Ionic and Coordination-Driven Self-Assembly. *Chem. Commun.* **2016**, *52*, 3388–3391.
- (38) Gilroy, J. B.; Patrick, B. O.; McDonald, R.; Hicks, R. G. Transition Metal Complexes of 3-Cyano- and 3-Nitroformazans. *Inorg. Chem.* **2008**, *47*, 1287–1294.
- (39) Hong, S.; Hill, L. M. R.; Gupta, A. K.; Naab, B. D.; Gilroy, J. B.; Hicks, R. G.; Cramer, C. J.; Tolman, W. B. Effects of Electron-Deficient β -Diketiminato and Formazan Supporting Ligands on Copper(I)-Mediated Dioxygen Activation. *Inorg. Chem.* **2009**, *48*, 4514–4523.
- (40) Chang, M.-C.; Dann, T.; Day, D. P.; Lutz, M.; Wildgoose, G. G.; Otten, E. The Formazanate Ligand as an Electron Reservoir: Bis(Formazanate) Zinc Complexes Isolated in Three Redox States. *Angew. Chem. Int. Ed.* **2014**, *53*, 4118–4122.
- (41) Travieso-Puente, R.; Chang, M.-C.; Otten, E. Alkali Metal Salts of Formazanate Ligands: Diverse Coordination Modes as a Result of the Nitrogen-Rich [NNCNN] Ligand Backbone. *Dalton Trans.* **2014**, *43*, 18035–18041.
- (42) Chang, M.-C.; Roewen, P.; Travieso-Puente, R.; Lutz, M.; Otten, E. Formazanate Ligands as Structurally Versatile, Redox-Active Analogues of β -Diketiminates in Zinc Chemistry. *Inorg. Chem.* **2015**, *54*, 379–388.

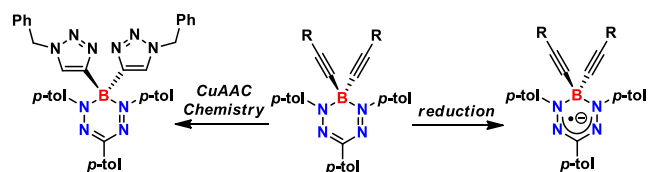
- (43) Mandal, A.; Schwederski, B.; Fiedler, J.; Kaim, W.; Lahiri, G. K. Evidence for Bidirectional Noninnocent Behavior of a Formazanate Ligand in Ruthenium Complexes. *Inorg. Chem.* **2015**, *54*, 8126–8135.
- (44) Protasenko, N. A.; Poddel'sky, A. I.; Bogomyakov, A. S.; Fukin, G. K.; Cherkasov, V. K. Heteroligand *o*-Semiquinonato-Formazanato Cobalt Complexes. *Inorg. Chem.* **2015**, *54*, 6078–6080.
- (45) Kabir, E.; Wu, C.-H.; Wu, J. I.-C.; Teets, T. S. Heteroleptic Complexes of Cyclometalated Platinum with Triarylformazanate Ligands. *Inorg. Chem.* **2016**, *55*, 956–963.
- (46) Travieso-Puente, R.; Broekman, J. O. P.; Chang, M.-C.; Demeshko, S.; Meyer, F.; Otten, E. Spin-Crossover in a Pseudo-tetrahedral Bis(formazanate) Iron Complex. *J. Am. Chem. Soc.* **2016**, *138*, 5503–5506.
- (47) Maar, R. R.; Rabiee Kenaree, A.; Zhang, R.; Tao, Y.; Katzman, B. D.; Staroverov, V. N.; Ding, Z. F.; Gilroy, J. B. Aluminum Complexes of $\text{N}_2\text{O}_2^{3-}$ Formazanate Ligands Supported by Phosphine Oxide Donors. *Inorg. Chem.* **2017**, *56*, 12436–12447.
- (48) Milocco, F.; Demeshko, S.; Meyer, F.; Otten, E. Ferrate(II) Complexes with Redox-Active Formazanate Ligands. *Dalton Trans.* **2018**, *47*, 8817–8823.
- (49) Maar, R. R.; Catingan, S. D.; Staroverov, V. N.; Gilroy, J. B. Formazanate Complexes of Hypervalent Group 14 Elements as Precursors to Electronically Stabilized Radicals. *Angew. Chem. Int. Ed.* **2018**, *57*, 9870–9874.
- (50) Broere, D. L. J.; Mercado, B. Q.; Lukens, J. T.; Vilbert, A. C.; Banerjee, G.; Lant, H. M. C.; Lee, S. H.; Bill, E.; Sproules, S.; Lancaster, K. M.; Holland, P. L. Reversible Ligand-Centered Reduction in Low-Coordinate Iron Formazanate Complexes. *Chem. Eur. J.* **2018**, *24*, 9417–9425.

- (51) Broere, D. L. J.; Mercado, B. Q.; Holland, P. L. Selective Conversion of CO₂ into Isocyanate by Low-Coordinate Iron Complexes. *Angew. Chem. Int. Ed.* **2018**, *57*, 6507–6511.
- (52) Kabir, E.; Patel, D.; Clark, K.; Teets, T. S. Spectroscopic and Electrochemical Properties of Electronically Modified Cycloplatinated Formazanate Complexes. *Inorg. Chem.* **2018**, *57*, 10906–10917.
- (53) Chang, M.-C.; Otten, E. Synthesis and Ligand-Based Reduction Chemistry of Boron Difluoride Complexes with Redox-Active Formazanate Ligands. *Chem. Commun.* **2014**, *50*, 7431–7433.
- (54) Barbon, S. M.; Reinkeluers, P. A.; Price, J. T.; Staroverov, V. N.; Gilroy, J. B. Structurally Tunable 3-Cyanoformazanate Boron Difluoride Dyes. *Chem. Eur. J.* **2014**, *20*, 11340–11344.
- (55) Barbon, S. M.; Staroverov, V. N.; Gilroy, J. B. Effect of Extended π Conjugation on the Spectroscopic and Electrochemical Properties of Boron Difluoride Formazanate Complexes. *J. Org. Chem.* **2015**, *80*, 5226–5235.
- (56) Maar, R. R.; Barbon, S. M.; Sharma, N.; Groom, H.; Luyt, L. G.; Gilroy, J. B. Evaluation of Anisole-Substituted Boron Difluoride Formazanate Complexes for Fluorescence Cell Imaging. *Chem. Eur. J.* **2015**, *21*, 15589–15599.
- (57) Maar, R. R.; Gilroy, J. B. Aggregation-Induced Emission Enhancement in Boron Difluoride Complexes of 3-Cyanoformazanates. *J. Mater. Chem. C.* **2016**, *4*, 6478–6482.
- (58) Chang, M.-C.; Chantzis, A.; Jacquemin, D.; Otten, E. Boron Difluorides with Formazanate Ligands: Redox-Switchable Fluorescent Dyes with Large Stokes Shifts. *Dalton Trans.* **2016**, *45*, 9477–9484.

- (59) Barbon, S. M.; Novoa, S.; Bender, D.; Groom, H.; Luyt, L. G.; Gilroy, J. B. Copper-Assisted Azide-Alkyne Cycloaddition Chemistry as a Tool for the Production of Emissive Boron Difluoride 3-Cyanoformazanates. *Org. Chem. Front.* **2017**, *4*, 178–190.
- (60) Hesari, M.; Barbon, S. M.; Staroverov, V. N.; Ding, Z.; Gilroy, J. B. Efficient Electrochemiluminescence of a Readily Accessible Boron Difluoride Formazanate Dye. *Chem. Commun.* **2015**, *51*, 3766–3769.
- (61) Hesari, M.; Barbon, S. M.; Mendes, R. B.; Staroverov, V. N.; Ding, Z.; Gilroy, J. B. Structural Tuning of Boron Difluoride Formazanate Electrochemiluminescence Mediated by Tri-*n*-propylamine. *J. Phys. Chem. C* **2018**, *122*, 1258–1266.
- (62) Chang, M.-C.; Otten, E. Reduction of (Formazanate)boron Difluoride Provides Evidence for an *N*-Heterocyclic B(I) Carbenoid Intermediate. *Inorg. Chem.* **2015**, *54*, 8656–8664.
- (63) Barbon, S. M.; Staroverov, V. N.; Gilroy, J. B. Structurally Diverse Boron-Nitrogen Heterocycles from an $\text{N}_2\text{O}_2^{3-}$ Formazanate Ligand. *Angew. Chem. Int. Ed.* **2017**, *56*, 8173–8177.
- (64) Barbon, S. M.; Gilroy, J. B. Boron Difluoride Formazanate Copolymers with 9,9-Di-*n*-Hexylfluorene Prepared by Copper-Catalyzed Alkyne-Azide Cycloaddition Chemistry. *Polym. Chem.* **2016**, *7*, 3589–3598.
- (65) Novoa, S.; Paquette, J. A.; Barbon, S. M.; Maar, R. R.; Gilroy, J. B. Side-Chain Boron Difluoride Formazanate Polymers via Ring-Opening Metathesis Polymerization. *J. Mater. Chem. C* **2016**, *4*, 3987–3994.
- (66) Novoa, S.; Gilroy, J. B. (Co)polymers Containing Boron Difluoride 3-Cyanoformazanate Complexes: Emission Enhancement via Random Copolymerization. *Polym. Chem.* **2017**, *8*, 5388–5395.

- (67) Dhindsa, J. S.; Maar, R. R.; Barbon, S. M.; Olivia Avilés, M.; Powell, Z. K.; Lagugné-Labarthe, F.; Gilroy, J. B. A π -Conjugated Inorganic Polymer Constructed from Boron Difluoride Formazanates and Platinum(II) Diynes. *Chem. Commun.* **2018**, *54*, 6899–6902.
- (68) Mondol, R.; Otten, E. Reactivity of Two-Electron-Reduced Boron Formazanate Compounds with Electrophiles: Facile N–H/N–C Bond Homolysis due to the Formation of Stable Ligand Radicals. *Inorg. Chem.* **2018**, *57*, 9720–9727.
- (69) Barbon, S. M.; Price, J. T.; Reinkeluers, P. A.; Gilroy, J. B. Substituent-Dependent Optical and Electrochemical Properties of Triarylformazanate Boron Difluoride Complexes. *Inorg. Chem.* **2014**, *53*, 10585–10593.
- (70) Gilroy, J. B.; McKinnon, S. D. J.; Koivisto, B. D.; Hicks, R. G. Electrochemical Studies of Verdazyl Radicals. *Org. Lett.* **2007**, *9*, 4837–4840.
- (71) Goze, C.; Ulrich, G.; Ziessel, R. Tetrahedral Boron Chemistry for the Preparation of Highly Efficient "Cascatelle" devices. *J. Org. Chem.* **2007**, *72*, 313–322.
- (72) Rumble, J. R., CRC Handbook of Chemistry and Physics, 98th Edition, CRC Press/Taylor and Francis, Boca Raton, FL.
- (73) Ziessel, R.; Goze, C.; Ulrich, G. Design and Synthesis of Alkyne-Substituted Boron in Dipyrrromethene Frameworks. *Synthesis* **2007**, 936–949.
- (74) Gilroy, J. B.; Ferguson, M. J.; McDonald, R.; Patrick, B. O.; Hicks, R. G. Formazans as β -Diketiminato Analogues. Structural Characterization of Boratetetrazines and their Reduction to Borataverdazyl Radical Anions. *Chem. Commun.* **2007**, 126–128.
- (75) Goze, C.; Ulrich, G.; Ziessel, R. Unusual Fluorescent Monomeric and Dimeric Dialkynyl Dipyrrromethene-Borane Complexes. *Org. Lett.* **2006**, *8*, 4445–4448.

For Table of Contents Only



Dialkynylborane complexes of formazanate ligands were generated from the corresponding boron difluoride complex. The alkyne substituents employed had little influence over low-energy UV-Vis absorption properties, but did affect redox potentials. The title complexes were converted to stable radical anions and copper-assisted alkyne-azide cycloaddition chemistry was used to elaborate structural diversity.